DISCRETE AND CONTINUOUS
DYNAMICAL SYSTEMS
Volume **17**, Number **3**, March **2007**

Website: http://aimSciences.org

pp. **203–221**

ON ULAM APPROXIMATION OF THE ISOLATED SPECTRUM AND EIGENFUNCTIONS OF HYPERBOLIC MAPS

Gary Froyland

School of Mathematics
University of New South Wales
Sydney NSW 2052, AUSTRALIA

(Communicated by Carlangelo Liverani)

Abstract. Perron-Frobenius operators and their eigendecompositions are increasingly being used as tools of global analysis for higher dimensional systems. The numerical computation of large, isolated eigenvalues and their corresponding eigenfunctions can reveal important persistent structures such as almost-invariant sets, however, often little can be said rigorously about such calculations. We attempt to explain some of the numerically observed behaviour by constructing a hyperbolic map with a Perron-Frobenius operator whose eigendecomposition is representative of numerical calculations for hyperbolic systems. We explicitly construct an eigenfunction associated with an isolated eigenvalue and prove that a special form of Ulam's method well approximates the isolated spectrum and eigenfunctions of this map.

1. **Introduction.** Perron-Frobenius operator (or transfer operator) methods are increasingly being used to solve problems arising in applications. Perron-Frobenius operators and their spectra have been very successful in the identification of molecular conformations [24]; transfer operators have enabled the detection of strange eigenmodes in fluid flow [21]; and Perron-Frobenius methods are being used to study the designs of office plans to ensure safe dispersal of airborne tracers such as smoke or radiation [20]. As Perron-Frobenius operators are a global representation of a system's dynamics, their spectra and eigenfunctions provide powerful tools of global analysis.

Let $T : M \circlearrowleft$ denote a discrete time dynamical system on a state space M, where for simplicity T is piecewise smooth and $M \subset \mathbb{R}^m$. Denote by $\mathcal{P} : \mathcal{B}(M) \circlearrowleft$, the Perron-Frobenius operator acting on a suitable space of real-valued functions (and distributions) on M. If $\mathcal{B}(M)$ is carefully chosen, the spectrum of the Perron-Frobenius operator is contained in the unit disk, and of particular interest in applications are the eigenfunctions corresponding to the eigenvalue 1 and other real eigenvalues close to 1.

Eigenfunctions of eigenvalues close to one represent *slowly decaying modes*. While at a microscopic scale, local expansion of T ensures rapid mixing, at a macroscopic scale, there are large structures determined by eigenfunctions corresponding to real

2000 *Mathematics Subject Classification.* Primary: 37M25, 37C30; Secondary: 37D20.

Key words and phrases. Perron-Frobenius operator, isolated spectrum, eigenfunction, almost-invariant set, Ulam's method, hyperbolic map.

Work partially supported by UNSW Faculty of Science Research Grant PS06898.

eigenvalues close to 1 that persist for a very long time. These structures are known as *almost-invariant sets* [9, 13].

Quasi-compactness of the Perron-Frobenius operator has been proven in a variety of settings [23, 16, 22, 5, 14, 2]. Quasi-compactness of $\mathcal{P} : \mathcal{B}(M) \circlearrowleft$ allows for the existence of a nontrivial isolated[1] spectrum, in particular, the existence of real eigenvalues close to 1. In the bounded variation setting, Baladi [1] produced an expanding Markov map of constant slope for which $\mathcal{P}$ had a complex-conjugate pair of isolated eigenvalues. In the same setting, Dellnitz *et al.* [8] described a parameterized family of expanding interval maps for which it was proven that the location of a nontrivial real, positive isolated eigenvalue may be controlled. For a C^2 expanding circle map with $\mathcal{P}$ acting on C^1 test functions, Keller and Rugh [17] proved the existence of an isolated eigenvalue with an analytic eigenfunction. In two-dimensions, Collet and Eckmann [7] construct a hyperbolic skew-product map with the expanding direction based upon the Baladi map [1], and show that Perron-Frobenius operator for this map inherits the complex-conjugate pair of eigenvalues from the one dimensional expanding dynamics.

When one constructs Ulam discretizations[2] [25, 19] of Perron-Frobenius operators of two-dimensional (non-uniformly) hyperbolic maps, it is common for numerical eigenfunctions corresponding to non-unit eigenvalues to have the appearance of being smooth along unstable manifolds and very rough along stable manifolds. For example, the eigenfunctions corresponding to the largest subunit real numerical eigenvalues for (i) the Standard map and (ii) Arnold's cat map are shown below in Figures 1 and 3. The dominant spectral values of the discretised Perron-Frobenius operators are shown in Figures 2 and 4. This behaviour has also been observed when, instead of discretizing via Ulam's method, finite dimensional approximations are constructed by truncating a complete function basis. Weber *et al.* [26] demonstrate this effect for a kicked top on the sphere, creating a finite-dimensional representation of $\mathcal{P}$ by truncating a spherical harmonic basis of $L^2([-1,1] \times S^1)$.

In order to better understand this behaviour, we construct a simple two-dimensional area preserving hyperbolic map that possesses a real, positive isolated eigenvalue. Moreover, we formally demonstrate that the corresponding eigenfunction has precisely the "smooth in unstable directions, rough in stable directions" behaviour that is numerically observed in many hyperbolic systems. We prove that Ulam's method accurately approximates both this eigenvalue and the associated eigenfunction when the Ulam partition sets are adapted to the unstable and stable dynamics.

The proof that Ulam's method well approximates the isolated spectrum and eigenfunction relies upon the ability to separate the unstable and stable directions into two one-dimensional problems. Therefore, the method of proof does not easily generalise to arbitrary hyperbolic maps; indeed counterexamples to spectral stability of the pure Ulam method have been recorded [4, 5]. Nevertheless, this partial result is to our knowledge the first positive demonstration that a pure[3] Ulam method

[1] We call ν an isolated eigenvalue if $\mathcal{P}\tilde{h} = \nu\tilde{h}$ and $|\nu|$ is strictly larger than the essential spectral radius of $\mathcal{P}$ for some nonzero $\tilde{h} \in \mathcal{B}(M)$. We will refer to $\tilde{h}$ as an isolated eigenfunction of $\mathcal{P}$.

[2] All Ulam matrices have been constructed using GAIO; http://www-math.uni-paderborn.de/∼agdellnitz/gaio/. All eigenvalue and eigenvector calculations have been performed in MATLAB.

[3] Blank *et al.* [5] prove that one achieves convergence of the isolated spectra and associated eigenfunctions as the Ulam partition sets decrease in diameter provided that the action of $\mathcal{P}$ is smoothed by noise of the order of (diameter of Ulam partition sets)$^{1/3}$. Unfortunately, Ulam's method is almost exclusively applied in practice without such smoothing considerations as these

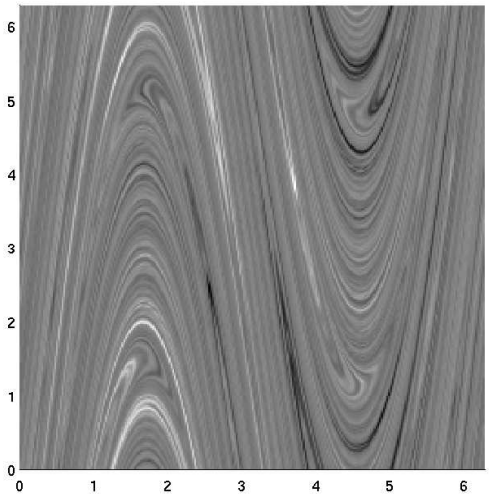

FIGURE 1. Ulam estimate of a "numerical eigenfunction" of the Perron-Frobenius operator of the Standard map $S : \mathbb{T}^2 \circlearrowleft$, $S(x, y) = (x + y, y + 8\sin(x + y)) \pmod{2\pi}$, corresponding to the numerical eigenvalue $\lambda \approx 0.7032$ (based on a 256×256 grid). The gray scale ranges from black, representing the minimum value of the eigenfunction to white, representing the maximum value of the eigenfunction.

can well approximate the isolated spectrum and eigenfunctions in a hyperbolic setting.

The outline of this paper is as follows. In §2 we give an informal geometric description of the map. In §3 we demonstrate via a simple argument that the isolated spectrum of $\mathcal{P}$ contains $1/2$. In §4 we construct the eigenfunction corresponding to $1/2$ and in §5 we demonstrate that a specialised pure Ulam method with partitions aligned to unstable and stable directions well approximates the isolated spectrum (consisting only of $1/2$ and 1) and the eigenfunction associated with $1/2$. Numerical results and conclusions are presented in §6. Additional proofs are given in §7.

2. **Geometric Description of an area preserving hyperbolic map.** We begin with a geometrical description of our two-dimensional map $T : [0, 1]^2 \circlearrowleft$ of the unit square. The action of T is shown in Figures 5, 6, and 7. The unit square is compressed uniformly in the x-direction by a factor of four and expanded uniformly in the y-direction by a factor of four; see Figure 6. This long, thin rectangle is then divided into eight vertical strips which are reassembled to form a unit square; see Figure 7. The bijective map T is area-preserving and uniformly hyperbolic. Because of the uniform expansion and compression by a factor of four, one might

would add considerably to the computational burden. Moreover, noise of this magnitude smooths away any fine structures in the eigenfunctions.

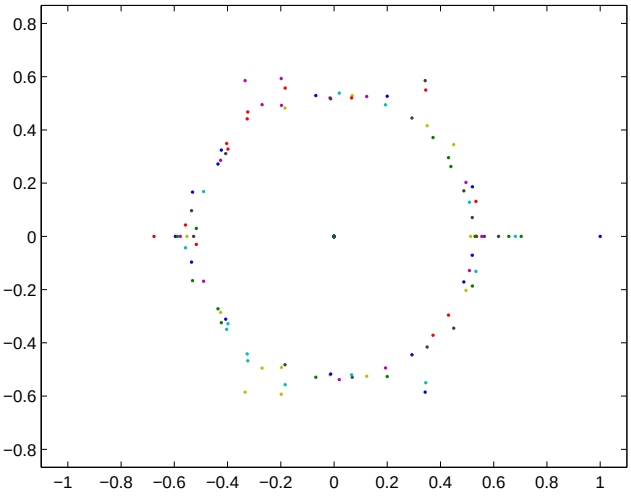

FIGURE 2. Largest 100 eigenvalues of an Ulam approximation of the Perron-Frobenius operator of the Standard map, numerically estimated using a 256×256 grid. The eigenfunction associated with the largest subunit positive real eigenvalue $\lambda \approx 0.7032$ is shown in Figure 1.

expect that the mixing rate, or decay of linear correlation between two observables is geometric with rate $1/4$. For many[4] observables, we will verify that this is true.

However, note that the left half of the unit square is almost preserved under one application of T; three-quarters of the left half remains in the left half. The same is true of the right half. Even though we have a stretching and compression of a factor of four at each iteration, there are some regions which do not mix at a rate commensurate with the local stretching. This behaviour can be explained by considering the eigendecomposition of the Perron-Frobenius operator of T.

3. **Existence of an isolated eigenvalue.** In this and the following section we define the Perron-Frobenius operator $\mathcal{P}$ (acting on suitable functions and distributions defined on $[0,1]^2$), demonstrate that $\mathcal{P}$ has an isolated eigenvalue $1/2$, and construct an eigendistribution $\tilde{h} : [0,1]^2 \to \mathbb{R}$ of $\mathcal{P}$ for this eigenvalue. Our Perron-Frobenius operator will act on a space of distributions that are smooth in the y-direction and rough in the x-direction. We use the functional analytic setup of [5]. The two main differences in settings between the present paper and [5] are firstly that we are working on the unit square rather than the 2-torus, and secondly that our space of regular functions used to define the distributions are allowed a discontinuity at $x = 1/2$. These two details are minor and are dealt with as required.

Let $0 < \beta < \gamma \leq 1$. We introduce the set of functions $\mathcal{D}_\beta$ which are β-Hölder in stable directions with Hölder constant 1, and with absolute value bounded by

[4] more precisely, there is a co-dimension 1 subspace of observables which decay at an exponential rate at close to $1/4$ or faster.

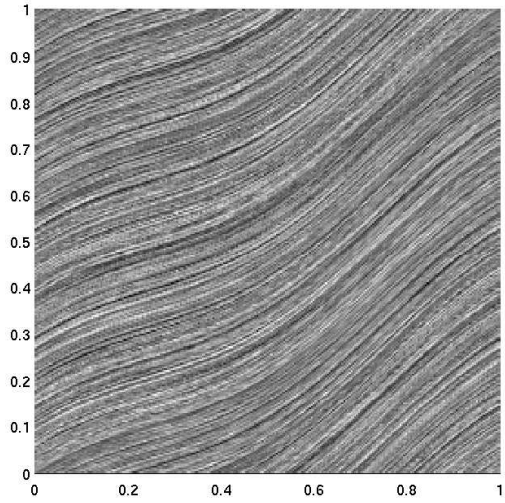

FIGURE 3. Ulam estimate of a "numerical eigenfunction" of the Perron-Frobenius operator of a smooth conjugacy of Anosov's cat map $C : \mathbb{T}^2 \circlearrowleft$, $C(x, y) = (2x + y, x + y) \pmod 1$, corresponding to the numerical eigenvalue $\lambda \approx 0.5538 + 0.01i$ (based on a 256×256 grid). For numerical stability in the eigenvalue computation, we have conjugated C with a diffeomorphism close to the identity. The gray scale ranges from black, representing the minimum value of the eigenfunction to white, representing the maximum value of the eigenfunction.

unity. Choose and fix some δ and define

$$\begin{aligned}\mathcal{D}_\beta \quad = \quad & \{\phi : [0,1]^2 \to \mathbb{R} : \phi \text{ measurable}, |\phi|_\infty \le 1, |\phi(x_1, y) - \phi(x_2, y)| \le |x_1 - x_2|^\beta \\ & \text{for } y \in [0,1], |x_1 - x_2| \le \delta, x_1, x_2 \in [0, 1/2) \text{ or } x_1, x_2 \in [1/2, 1]\}. \quad (1)\end{aligned}$$

This is the class of regular functions we will use to define our distributions. Note that the β-Hölderness is measured only for x_1, x_2 pairs in LHS and RHS of the unit square, allowing breaks in Hölder continuity across the line $x = 1/2$.

For $h \in C^1([0,1]^2, \mathbb{R})$, and some fixed constant $b > 0$, let

$$\|h\|_s := \sup_{\phi \in \mathcal{D}_\beta} \int_{[0,1]^2} h\phi \, dm, \quad (2)$$

$$\|h\|_u := \int_{[0,1]^2} \frac{\partial h}{\partial y} \, dm, \quad (3)$$

$$\|h\| := \|h\|_u + b\|h\|_s, \quad (4)$$

$$\|h\|_w := \sup_{\phi \in \mathcal{D}_\gamma} \int_{[0,1]^2} h\phi \, dm, \quad (5)$$

where m is normalized Lebesgue measure on $[0,1]^2$. The norm $\|\cdot\|_s$ is a (weak) measure of roughness in the stable directions, while $\|\cdot\|_u$ measures roughness in a stronger sense in the unstable direction. The norm $\|\cdot\|$ combines $\|\cdot\|_s$ and $\|\cdot\|_u$,

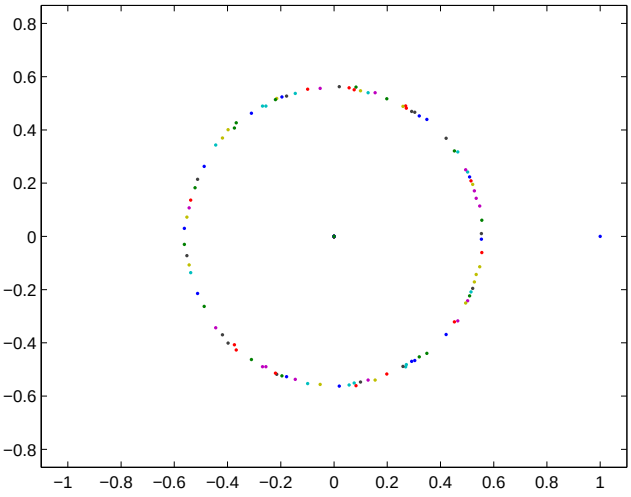

FIGURE 4. Largest 100 eigenvalues of an Ulam approximation of the Perron-Frobenius operator of Anosov's cat map, numerically estimated using a 256×256 grid. The eigenfunction associated with the largest subunit "most positive" real eigenvalue $\lambda \approx 0.5538 + 0.01i$ is shown in Figure 3. Note that the numerics display no obvious isolated eigenvalue, consistent with the proof of an empty isolated spectrum for linear toral automorphisms; see Example 2.2.6 [5].

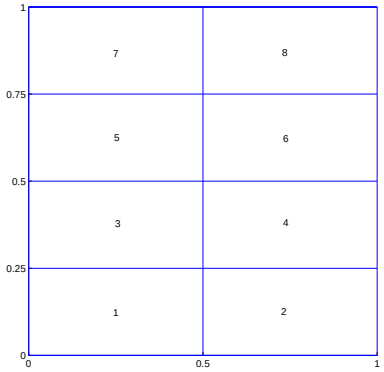

FIGURE 5. Initial state of the unit square.

while $\|\cdot\|_w$ is a weaker form of $\|\cdot\|_s$ to be used for technical purposes. Let $\mathcal{B}([0,1]^2)$ and $\mathcal{B}_w([0,1]^2)$ denote the completions of $C^1([0,1]^2,\mathbb{R})$ with respect to the norms $\|\cdot\|$ and $\|\cdot\|_w$ respectively. The action of $\mathcal{P}$ on C^1 extends continuously to $\mathcal{B}([0,1]^2)$ and $\mathcal{B}_w([0,1]^2)$.

Lemma 1. *$\mathcal{B}([0,1]^2)$ may be compactly embedded in $\mathcal{B}_w([0,1]^2)$.*

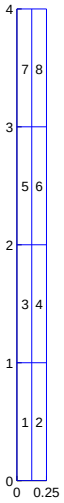

FIGURE 6. Intermediate state of the unit square under the action of T.

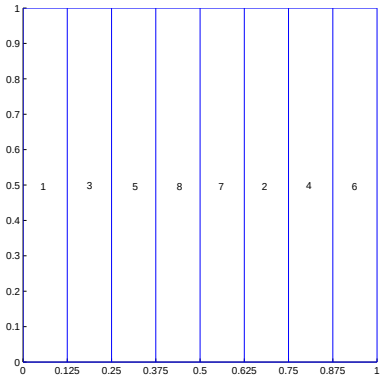

FIGURE 7. Final state of the unit square under the action of T.

This result is proven in Proposition 2.2.2 [5]. The setting here is slightly different as we work on a square instead of a 2-torus and $\mathcal{D}_\beta$ allows breaks in β-Hölderness at $x = 1/2$. The details of the proof of Proposition 2.2.2 [5] (in particular Lemma 3.6.2 [5]) can be followed through to check that Lemma 1 holds in the current setting.

Proposition 1. *$\mathcal{P} : \mathcal{B}([0,1]^2) \circlearrowleft$, is quasi-compact, and has an essential spectral radius bounded by $1/4^\beta$.*

Proof. Proposition 1 is almost an application of Theorem 1 [5]. Theorem 1 [5] applies to C^3 hyperbolic maps on $\mathbb{T}^2$, while our example map T is only piecewise smooth and acts on $[0,1]^2$. One needs to verify that the conclusion of Lemma 2.2.1 [5] holds; namely that a Lasota-Yorke inequality can be developed. Because of the uniform stretching and compression of the map T, verifying the existence of such an inequality is routine and we leave the details to the reader. Theorem 1 [5] states

that the essential spectral radius of $\mathcal{P}$ is bounded by $\sigma > \max\{1/4, 1/4^\beta\}$. This yields the statement in Proposition 1. □

Theorem 1. *For $1/2 < \beta < 1$, $\mathcal{P} : \mathcal{B}([0,1]^2) \circlearrowleft$ possesses an isolated eigenvalue 1/2.*

Proof. Define $h_0 : [0,1]^2 \to \mathbb{R}$ by $h_0(x,y) = \begin{cases} 1, & \text{if } x < 1/2; \\ -1, & \text{otherwise.} \end{cases}$ Then $\int_{[0,1]^2} h_0 \cdot h_0 \circ T^n \, dm = 1/2^n$, as the action of T on the sets $\{x < 1/2\}$ and $\{x \geq 1/2\}$ is that of a Markov chain governed by $\begin{pmatrix} 3/4 & 1/4 \\ 1/4 & 3/4 \end{pmatrix}$. Hence, $\int_{[0,1]^2} \mathcal{P}^n h_0 \cdot h_0 \, dm = 1/2^n$. Let $1/4^\beta < r < 1/2$. Quasi-compactness of $\mathcal{P}$ tells us that $\mathcal{P} = \sum_{i=1}^k \lambda_i \Pi_{\lambda_i} + \Psi$, where $\lambda_1, \ldots, \lambda_k$ denote the eigenvalues of $\mathcal{P}$ with moduli larger than r, Π_{λ_i} denote the corresponding projections onto eigenspaces, and $\|\Psi^n\| \leq Hr^n$ for some constant $H > 0$. Since $\int_{[0,1]^2} \mathcal{P}^n h_0 \cdot h_0 \, dm = 1/2^n$ and $\|\Psi^n\|_w \leq \|\Psi^n\| \leq Hr^n$, we must have that $1/2 = \lambda_i$ for some $i = 1, \ldots, k$. □

4. **Construction of an isolated eigendistribution.** One may obtain the eigendistribution of $\mathcal{P}$ corresponding to the isolated eigenvalue 1/2 via $\Pi_{1/2}$, the spectral projection for the eigenvalue 1/2. In this section, we construct this eigendistribution explicitly as the machinery we develop will be used in subsequent sections. Because our map is bijective and area preserving, the Perron-Frobenius operator may be written as

$$\mathcal{P}h(x,y) = h(T^{-1}(x,y)). \tag{6}$$

The inverse of T is explicitly given by

$$T^{-1}(x,y) = \begin{cases} (4x, y/4), & x \in [0,1/8); \\ (4(x-1/8), y/4 + 1/4), & x \in [1/8,1/4); \\ (4(x-1/4), y/4 + 1/2), & x \in [1/4,3/8); \\ (4(x-3/8) + 1/2, y/4 + 3/4), & x \in [3/8,1/2); \\ (4(x-1/2), y/4 + 3/4), & x \in [1/2,5/8); \\ (4(x-5/8) + 1/2, y/4), & x \in [5/8,3/4); \\ (4(x-3/4) + 1/2, y/4 + 1/4), & x \in [3/4,7/8); \\ (4(x-7/8) + 1/2, y/4 + 1/2), & x \in [7/8,1]. \end{cases} \tag{7}$$

We will make use of the fact[5] that

$$\mathcal{P}(\mathbf{1}(y)g(x)) = \mathbf{1}(y)g(T_s(x)), \tag{8}$$

where T_s is the piecewise linear interval map defined below.

$$T_s(x) = \begin{cases} 4x, & x \in [0,1/8); \\ 4x - 1/2, & x \in [1/8,1/4); \\ 4x - 1, & x \in [1/4,1/2); \\ 4x - 2, & x \in [1/2,3/4); \\ 4x - 5/2, & x \in [3/4,7/8); \\ 4x - 3, & x \in [7/8,1]. \end{cases} \tag{9}$$

[5]A similar observation is used in [15], where eigenfunctions for the Perron-Frobenius operators of both the Bernoulli (circle-doubling) map and the standard Baker's map are explicitly constructed in an L^2 setting.

Let

$$\mathcal{D}_{\beta,1} = \{f : [0,1] \to \mathbb{R} : f \text{ measurable}, |f|_\infty \le 1, |f(x_1) - f(x_2)|/|x_1 - x_2|^\beta \le 1, \\ x_1, x_2 \in [0, 1/2) \text{ or } x_1, x_2 \in [1/2, 1]\}.$$

Introduce the norm

$$\|g\|_{s,1} = \sup_{f \in \mathcal{D}_{\beta,1}} \int g \cdot f \, dm. \tag{10}$$

Define $\mathcal{B}([0,1])$ to be the completion of $C^1([0,1])$ with respect to $\|\cdot\|_{s,1}$. Introduce the Koopman operator $U_s : \mathcal{B}([0,1]) \circlearrowleft$, defined by $U_s g = g \circ T_s$ for $g \in C^1([0,1], \mathbb{R})$, and the action of U_s extended continuously to $g \in \mathcal{B}([0,1])$.

Lemma 2. *Define* $g_0 : [0,1] \to \mathbb{R}$ *by*

$$g_0 = \begin{cases} 1, & x \in [0, 1/2); \\ -1, & x \in [1/2, 1], \end{cases} \tag{11}$$

$g_n : [0,1] \to \mathbb{R}$ *by*

$$g_n = 2^n U_s^n g_0, \tag{12}$$

and $\tilde{g} = \lim_{n\to\infty} g_n$. *Then* $\tilde{g}$ *is a nonzero element of* $\mathcal{B}([0,1])$ *satisfying* $U_s \tilde{g} = \tilde{g}/2$.

Proof. See proofs section. □

The graphs of g_0, g_1, and g_2 are displayed in Figure 8.

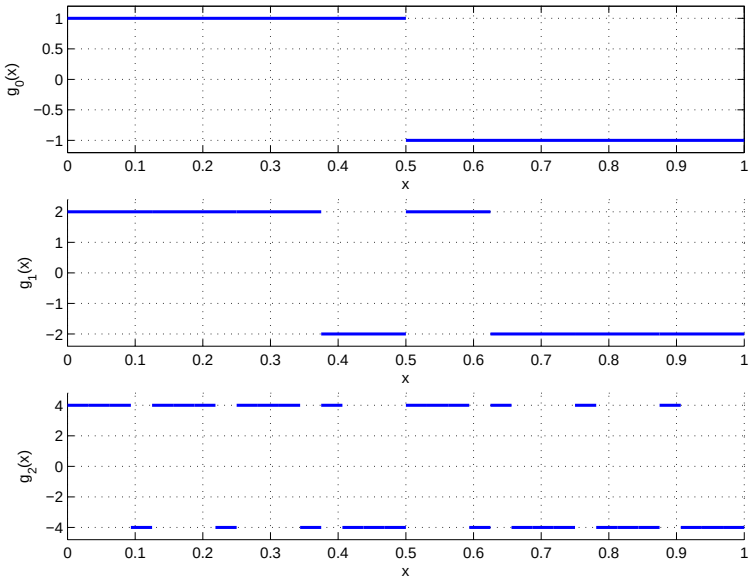

FIGURE 8. Graphs of g_0, g_1, g_2 as labelled.

Theorem 2. *Define* g_n *as in (12). Under the conditions of Theorem 1,* $\mathcal{P} : \mathcal{B}([0,1]^2) \circlearrowleft$ *possesses an isolated eigenvalue 1/2 and the corresponding eigendistribution is* $\tilde{h} = \lim_{n\to\infty} h_n$ *where* $h_n(x,y) = g_n(x)$.

Proof. The proof mimics the proof of Lemma 2. Using the norms (2), (3), and (4), we show that $\tilde{h} = \lim_n h_n$ is a nonzero element of $\mathcal{B}([0,1]^2)$. To show that $\mathcal{P}\tilde{h} = \tilde{h}/2$, we use the fact that $\|U_s g_n - g_n/2\|_{s,1} \to 0$ as $n \to \infty$. By straightforward computation, $\mathcal{P}(h_n(x,y)) = \mathcal{P}(\mathbf{1}(y)g_n(x)) = \mathbf{1}(y)(U_s g_n(x))$. Thus

$$\begin{aligned}
\|\mathcal{P}h_n - h_n/2\| &= \|\mathbf{1}(y)(U_s g_n(x)) - \mathbf{1}(y)g_n(x)/2\| \\
&= \|\mathbf{1}(y)(U_s g_n(x)) - \mathbf{1}(y)g_n(x)/2\|_u \\
&\quad + b\|\mathbf{1}(y)(U_s g_n(x)) - \mathbf{1}(y)g_n(x)/2\|_s \\
&= 0 + b\|U_s g_n(x) - g_n(x)/2\|_{s,1} \\
&\to 0 \qquad \text{as in the proof of Lemma 2.}
\end{aligned}$$

□

5. **Description of Ulam approximation.** We construct via Ulam's method a finite-dimensional approximation of the operator $\mathcal{P} : \mathcal{B}([0,1]^2) \circlearrowleft$. Typically, one constructs a sequence of partitions $\mathfrak{P}_n = \{A_1, \ldots, A_{R(n)}\}$ of $[0,1]^2$ comprised of regular partition sets with $\max_{1\le i\le R(n)} \operatorname{diam}(A_i) \to 0$ as $n \to \infty$. For a given n, an Ulam matrix $P_{n,ij} := m(A_i \cap T^{-1}A_j)/m(A_i)$ and its left fixed eigenvector $p_n = [p_{n,1}, \ldots, p_{n,R(n)}]$ are computed, the latter normalized so that $\sum_{i=1}^{R(n)} p_{n,i} = 1$. In various settings [19, 11, 10, 9, 5] one can show that the sequence of probability measures $\mu_n(B) := \sum_{i=1}^{R(n)} p_{n,i} m(B \cap A_i)$ converges to an absolutely continuous or Sinai-Bowen-Ruelle measure. In the present paper we make use of Ulam's method to approximate eigenfunctions that are not fixed, but rather correspond to real eigenvalues close to 1.

For piecewise smooth expanding interval maps without periodic turning points, Blank and Keller [4] show that the isolated spectrum is stable under certain stochastic perturbations, including the Ulam approximation. This work extended a similar result [3] for convolution-type perturbations, which do not include Ulam-type approximations. In the two-dimensional Anosov setting, the author [12] demonstrated that if the Ulam matrix is constructed using a Markov partition, then Ulam's method well approximated the isolated spectrum and the associated eigenfunctions of the induced expanding map on unstable foliations. In Theorem 3 below, for the map T from §2 we prove convergence of the eigenfunctions on the full space, not just on unstable foliations. In [5] a similar result is shown for reasonably general partitions when the Ulam construction is applied to a highly smoothed (relative to the partition sets) version of $\mathcal{P}$. Theorem 3 uses a pure Ulam method, without smoothing. The map T described in §2 allows us to separate the unstable and stable dynamics. We prove convergence of the numerical estimates of the dominant subunit eigendistribution in the $\|\cdot\|$ norm. Our main result is:

Theorem 3. *Let* $\{I_1, \ldots, I_{P(n)}\} := \bigvee_{k=0}^{n} T_s^{-k}\mathfrak{P}_0$ *where*

$$\mathfrak{P}_0 = \{[0,1/8), [1/8,2/8), \ldots, [7/8,1]\}$$

and T_s *is defined as in (9). Let* $\{J_1, \ldots, J_{Q(n)}\}$ *be a partition of the unit interval. Partition the unit square via*

$$\{I_p \times J_q\}_{p=1,\ldots,P(n);q=1,\ldots,Q(n)} := \{A_i\}_{i=1,\ldots,P(n)Q(n)}.$$

Assume that $\max_{1\le i\le P(n)Q(n)} \operatorname{diam}(A_i) \to 0$ *as* $n \to \infty$. *Construct*

$$P_{n,ij} = \frac{m(A_i \cap T^{-1}A_j)}{m(A_i)}, \tag{13}$$

where m is normalized Lebesgue measure and T is defined as in §2. Compute the left eigenvector v_n corresponding to the eigenvalue $1/2$ and construct the function $\hat{h}_n(x,y) := \sum_{i=1}^{P(n)Q(n)} v_{n,i}\chi_{A_i}(x,y)$. If v_n is suitably normalized, then $\hat{h}_n(x) = h_n(x)$, and thus $\|\hat{h}_n - \tilde{h}\| \to 0$ as $n \to \infty$, where h_n and $\tilde{h}$ are defined in Theorem 2.

Proof. See §7. □

6. **Numerical results and conclusions.** We have constructed a hyperbolic map of the unit square whose Perron-Frobenius operator possesses an isolated eigenvalue. Further, we have proven that Ulam's method, applied using a partition that is adapted to the stable and unstable directions successfully approximates both this isolated eigenvalue and its corresponding eigendistribution. Below we report on numerical calculations performed on a 128×128 grid $\mathfrak{P}_3$ aligned to the coordinate axes. Figure 9 shows the largest 100 numerical eigenvalues of P_3. The numerical eigenvalue $\lambda_3 = 0.5108$ approximates the eigenvalue $1/2$, the existence of which was demonstrated in Theorem 1. The Ulam estimate $\hat{h}_3$ of the isolated eigendistribution $\tilde{h}$ is shown in Figure 10. This numerical eigenfunction very clearly displays the roughness in the stable direction and smoothness in the unstable direction discussed earlier. Moreover, Theorem 3 guarantees that the numerical eigenfunctions computed using Ulam's method will converge in the $\|\cdot\|$ norm to the isolated

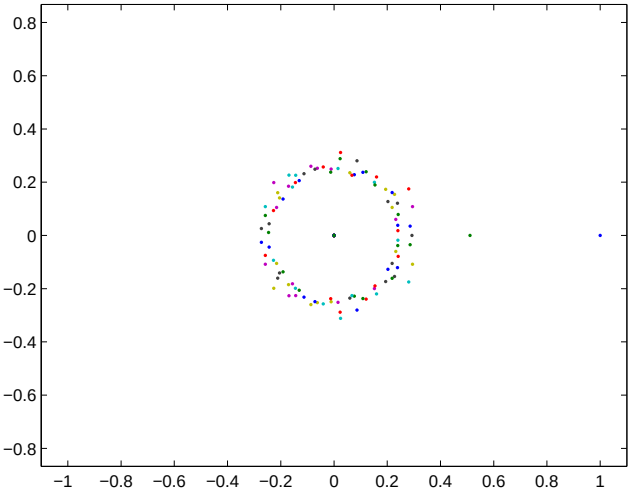

FIGURE 9. Largest 100 eigenvalues of the Perron-Frobenius operator of the map T from §2, numerically estimated from an Ulam approximation on the 128×128 grid $\mathfrak{P}_3$. The numerical eigenfunction for the largest subunit positive real eigenvalue $\lambda \approx 0.5108$ is shown in Figure 10. The small deviation of the numerically computed eigenvalue from $1/2$ is due to numerical issues. Lebesgue measure is approximated by 961 sample points per grid set and the MATLAB eigenvalue routines have a finite accuracy tolerance.

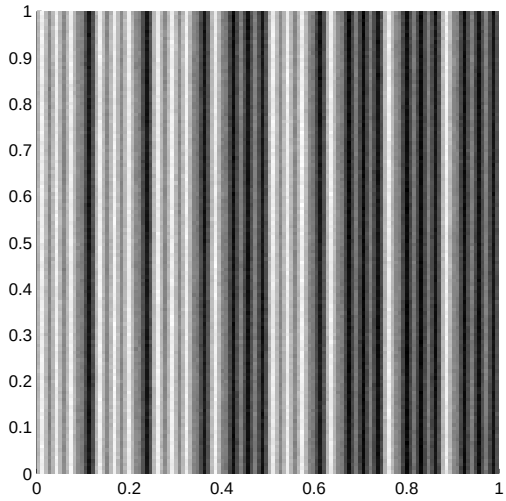

FIGURE 10. Ulam estimate of the eigendistribution $\tilde{h}$ of the Perron-Frobenius operator of $T : [0,1]^2 \circlearrowleft$ as defined in §2, corresponding to the numerical eigenvalue $\lambda \approx 0.5108$. The gray scale ranges from black, representing the minimum value of the eigenfunction to white, representing the maximum value of the eigenfunction.

eigendistribution $\tilde{h}$. To our knowledge this is the first such positive proof that a pure Ulam's method can approximate the isolated spectrum and eigendistributions of hyperbolic maps on the full state space.

Counterexamples to Ulam's method reproducing the subunit spectrum have been reported in [4, 5] for Anosov's cat map C. In [5] it is demonstrated that the Perron-Frobenius operator for C (acting on $\mathcal{B}(\mathbb{T}^2)$) has empty isolated spectrum, while [4, 5] detail a combination of theoretical and numerical evidence showing that Ulam matrices based upon several different partitions not aligned to the stable and unstable directions have large "fake" eigenvalues that lie outside the disk $|z| \leq 1/\lambda_u$, where λ_u is the largest eigenvalue of the matrix $\begin{pmatrix} 2 & 1 \\ 1 & 1 \end{pmatrix}$. In contrast, Brini *et al.* [6] demonstrate that for Anosov's cat map, an Ulam matrix based upon a Markov partition recovers the "correct" mixing rate of $1/\lambda_u$. The strength of the counterexamples in [4, 5] is weakened by the fact [5] that the Perron-Frobenius operators of linear toral automorphisms do not have subunit isolated spectra to approximate when $\mathcal{P}$ acts on $\mathcal{B}(\mathbb{T}^2)$. One might argue that it is unreasonable to expect a finite-dimensional approximation such as Ulam's method to correctly reproduce the non-isolated spectrum.

Pursuing this line of argument, we describe a numerical experiment for the map T from §2, which we have shown *does* possess a subunit isolated eigenvalue. We conjugate T with C to obtain $\tilde{T} = C^{-1} \circ T \circ C$. Using the partition $\mathfrak{P}_3$ we compute the Ulam approximation $\tilde{P}_3$ to $\tilde{\mathcal{P}}$, the Perron-Frobenius operator for $\tilde{T}$. As C preserves Lebesgue measure, $\tilde{P}_3$ computed on $\mathfrak{P}_3$ equals P_3 computed on the

partition $C(\mathfrak{P}_3)$; this latter partition is now no longer aligned with the stable and unstable directions of T. Thus by computing $\tilde{P}_3$ on $\mathfrak{P}_3$ we achieve the effect of computing P_3 on $C(\mathfrak{P}_3)$. The largest 100 eigenvalues of $\tilde{P}_3$ are shown in Figure 11. The second largest eigenvalue of $\tilde{P}_3$ is 0.4989, reproducing very well the eigenvalue

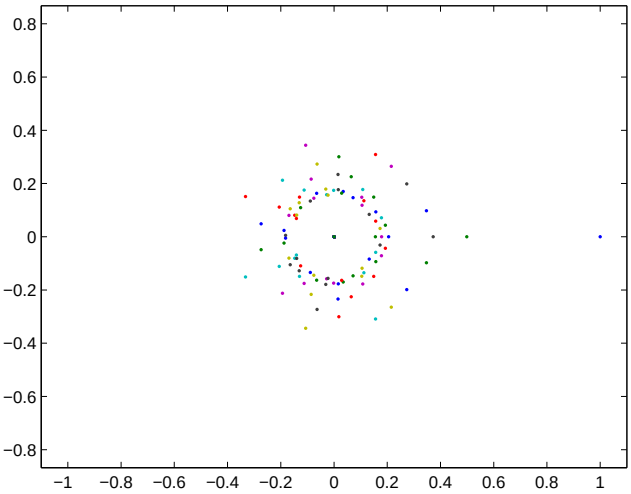

FIGURE 11. Largest 100 eigenvalues of the Perron-Frobenius operator of $\tilde{T} = C^{-1} \circ T \circ C$, numerically estimated from an Ulam approximation on the 128×128 grid $\mathfrak{P}_3$. The numerical eigenfunction for the largest subunit positive real eigenvalue $\lambda \approx 0.4989$ is shown in Figure 10. The small deviation of the numerically computed eigenvalue from $1/2$ is due to numerical issues. Lebesgue measure is approximated by 961 sample points per grid set and the MATLAB eigenvalue routines have a finite accuracy tolerance.

$1/2$ of $\tilde{\mathcal{P}}$ (and $\mathcal{P}$). Comparing Figures 9 and 11, we note that location of the third largest eigenvalue has moved outwards, but the second largest eigenvalue (in fact, in this case, the entire isolated spectrum of $\mathcal{P}$) has remained relatively unchanged. Thus, while the isolated spectrum is well approximated, the spectral calculations in Figures 9 and 11 also display the "fake" eigenvalues reported in [4, 5]. This suggests that Ulam approximations accurately reproduce, at least in a partial sense, the non-isolated spectrum only in very special circumstances such as those outlined in [6].

Turning now to the estimate of the isolated eigendistribution, since $\mathcal{P}\tilde{h} = \tilde{h}/2$, we have $\tilde{\mathcal{P}}(\tilde{h} \circ C) = (\tilde{h} \circ C)/2$. Thus we expect the eigendistribution $\tilde{h} \circ C$ to be smooth in directions $C^{-1}W^u$, where W^u is the unstable direction for T, and rough in directions $C^{-1}W^s$, where W^s is the stable direction for T. These features are clearly seen in Figure 12. This experiment represents one positive example where it *appears* numerically that the subunit isolated spectrum and corresponding eigendistribution can be approximated by a pure Ulam's method even when the partition sets are not adapted to the stable and unstable directions.

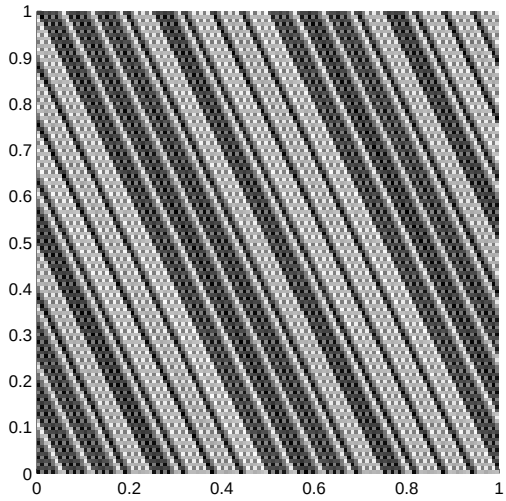

FIGURE 12. Ulam estimate of an eigenfunction of the Perron-Frobenius operator of $\tilde{T} = C^{-1} \circ T \circ C$, corresponding to the numerical eigenvalue $\lambda \approx 0.4989$. The gray scale ranges from black, representing the minimum value of the eigenfunction to white, representing the maximum value of the eigenfunction.

Remark 1. An extension of property (8) is as follows. Call the Perron-Frobenius operator of a map of the unit square $(\mathcal{F}, \mathcal{G})$-*separable* if there are piecewise smooth maps $T_u, T_s : [0,1] \circlearrowleft$ such that $\mathcal{P}_u$ is the Perron-Frobenius operator of T_u, U_s is the Koopman operator of T_s, and

$$\mathcal{P}(f(y)g(x)) = (\mathcal{P}_u f)(y)(U_s g)(x) \tag{14}$$

for $f \in \mathcal{F} \subset L^1([0,1], m)$ and $g \in \mathcal{G} \subset \mathcal{B}([0,1])$. For example, the map T from §2 is $(\mathcal{F}, \mathcal{G})$-separable for $\mathcal{G} = \mathcal{B}([0,1])$ and $\mathcal{F} = \{f \in L^1\colon\ f(y) = f(y + 1/4), 0 \le y < 3/4\}$. Approximation results such as Theorem 3 might be constructed for isolated eigendistributions $h(x,y) = f(y)g(x)$ where $f \in \mathcal{F}, g \in \mathcal{G}$ and $\mathcal{P}$ is $(\mathcal{F}, \mathcal{G})$ separable.

As described in the introduction, Perron-Frobenius based numerical methods are increasingly being used in applications. Theorems 2 and 3 are a step towards formalizing these calculations for multidimensional hyperbolic systems. While the piecewise smooth map T we have used clearly illustrates the features we wished to draw out, the question of whether there exists a smooth hyperbolic map with subunit isolated spectrum is to our knowledge still an open one. Extending Theorem 3 to more general partitions is very desirable, however the way forward is not clear and the existence of examples that have poor approximation properties makes it likely that a careful selection of hypotheses will be required to guarantee a positive result for a pure Ulam's method. Despite these difficulties, we believe that a greater formal and numerical understanding of the information contained in the eigendecomposition of $\mathcal{P}$ can lead to powerful methods of analyzing global system properties.

7. **Proofs.** First, two technical lemmas.

Lemma 3. *Let $f \in \mathcal{D}_{\beta,1}$ and $g \in \mathcal{B}([0,1])$. Then $\int_{[0,1]} U_s g \cdot f \, dm = \int_{[0,1]} g \cdot \mathcal{P}_s f \, dm$*

Proof. $g \in \mathcal{B}([0,1])$ implies there is $g_m \in C^1$ such that $\|g_n - g_m\|_{s,1} \to 0$, that is, $\lim_{m,n} \sup_{f \in \mathcal{D}_{\beta,1}} \int (g_n \cdot f - g_m \cdot f) \, dm = 0$. We define $U_s g$ via the limit of a smoothing of $U_s g_m$ (we need to smooth the $U_s g_m$ as they are only piecewise C^1). For brevity, neglecting the smoothing, as it plays no real role,

$$\begin{aligned}
\int_{[0,1]} U_s g \cdot f \, dm &:= \lim_m \int_{[0,1]} g_m \circ T_s \cdot f \, dm \\
&= \lim_m \int_{[0,1]} g_m \cdot \mathcal{P}_s f \, dm \qquad \text{(see, for example, p.48 [18])} \\
&:= \int_{[0,1]} g \cdot \mathcal{P}_s f \, dm
\end{aligned}$$

□

Lemma 4. $\|U_s\|_{s,1} = 1$.

Proof. We first prove that $\|U_s\|_{s,1} \leq 1$.

$$\begin{aligned}
\|U_s\|_{s,1} &= \sup_{g \in \mathcal{B}([0,1]), \|g\|_{s,1} \leq 1} \sup_{f \in \mathcal{D}_{\beta,1}} \int_{[0,1]} U_s g \cdot f \, dm \qquad (15) \\
&= \sup_{g \in \mathcal{B}([0,1]), \|g\|_{s,1} \leq 1} \sup_{f \in \mathcal{D}_{\beta,1}} \int_{[0,1]} g \cdot \mathcal{P}_s f \, dm \quad \text{by Lemma 3,} \\
&\leq \sup_{g \in \mathcal{B}([0,1]), \|g\|_{s,1} \leq 1} \sup_{f \in \mathcal{D}_{\beta,1}} \int_{[0,1]} g \cdot f \, dm \qquad \text{as } \mathcal{P}_s f \in \mathcal{D}_{\beta,1}, \\
&= 1
\end{aligned}$$

By choosing $g = f \equiv 1$ in (15), we see that $\|U_s\|_{s,1} = 1$. □

Proof of Lemma 2.

1. To show $\tilde{g} \in \mathcal{B}([0,1])$ is relatively straightforward. One may show that standard C^1 smoothings of g_n form a $\|\cdot\|_{s,1}$-Cauchy sequence and by completeness, the limit $\tilde{g} \in \mathcal{B}([0,1])$.
2. To show $\tilde{g} \neq 0$ one may directly compute the limit of the norms $\|g_n\|_{s,1}$ and verify that this limit is 1.
3. To show $U_s \tilde{g} = \tilde{g}/2$, we demonstrate that $\|U_s g_n - g_n/2\|_{s,1} \to 0$ as $n \to \infty$. We need to show that $\lim_{n\to\infty} \sup_{f \in \mathcal{D}_{\beta,1}} \int_{[0,1]} (U_s g_n(x) - g_n(x)/2) f(x) \, dx = 0$. First, some rewriting:

$$\begin{aligned}
&\lim_{n\to\infty} \sup_{f \in \mathcal{D}_{\beta,1}} \int_{[0,1]} (U_s g_n(x) - g_n(x)/2) f(x) \, dx \\
= &\lim_{n\to\infty} \sup_{f \in \mathcal{D}_{\beta,1}} \int_{[0,1]} (2^n U_s^{n+1} g_0(x) - 2^n U_s^n g_0(x)/2) f(x) \, dx \\
= &\lim_{n\to\infty} 2^n \sup_{f \in \mathcal{D}_{\beta,1}} \int_{[0,1]} (U_s g_0(x) - g_0(x)/2) \mathcal{P}_s^n f(x) \, dx \qquad \text{by Lemma 3 (16)}
\end{aligned}$$

Let

$$\begin{aligned}
\bar{\mathcal{D}}_{\beta,1} = \{f : [0,1] \to \mathbb{R} : f \text{ measurable}, |f|_\infty < \infty, \\
|f(x_1) - f(x_2)| / |x_1 - x_2|^\beta < \infty, x_1, x_2 \in [0, 1/2) \text{ or } x_1, x_2 \in [1/2, 1]\}.
\end{aligned}$$

Define $\|f\|_{\beta,1} = |f|_\infty + \max\{|f_{|[0,1/2]}|_\beta, |f_{|(1/2,1]}|_\beta\}$, where $|\cdot|_\beta$ is the standard β-Hölder seminorm. It is relatively straightforward to demonstrate that $\mathcal{P}_s : (\bar{\mathcal{D}}_{\beta,1}, \|\cdot\|_{\beta,1}) \circlearrowleft$, the Perron-Frobenius operator for T_s, is quasi-compact with essential spectral radius bounded by $1/4^\beta$. Furthermore, the only spectral values outside $|z| \le 4^{-\beta}$ are $1/2$ and 1, both with unit multiplicity. Thus we have the $\mathcal{P}_s$-invariant decomposition

$$\bar{\mathcal{D}}_{\beta,1} = \mathrm{sp}\{\mathbf{1}\} \oplus \mathrm{sp}\{g_0\} \oplus \tilde{\mathcal{D}}_{\beta,1},$$

where $\tilde{\mathcal{D}}_{\beta,1}$ corresponds to the essential spectrum. Thus any $f \in \bar{\mathcal{D}}_{\beta,1}$ may be written as $f = a_{\mathbf{1}}(f)\mathbf{1} + a_0(f)g_0 + f_1$ where $f_1 \in \tilde{\mathcal{D}}_{\beta,1}$ and $a_{\mathbf{1}}(f), a_0(f)$, are uniquely determined. As $\int_{[0,1]} g_n \, dx = 0$ for each $n \ge 0$, without loss, we can assume that $\int_{[0,1]} f \, dx = 0$; thus $a_{\mathbf{1}}(f) = 0$. We demonstrate below that (16)=0 by separating the two cases.

(a) $f \in \mathrm{sp}\{g_0\}$:

$$\begin{aligned}(16) &= \lim_{n\to\infty} 2^n \int_{[0,1]} (U_s g_0(x) - g_0(x)/2) 2^{-n} g_0(x) \, dx \\ &= \int_{[0,1]} (U_s g_0(x) - g_0(x)/2) g_0 \, dx = 0\end{aligned}$$

by direct computation.

(b) $f \in \tilde{\mathcal{D}}_{\beta,1}$

$$\begin{aligned}(16) &\le \lim_{n\to\infty} 2^n \sup_{f\in\tilde{\mathcal{D}}_{\beta,1}} \int_{[0,1]} (U_s g_0 - g_0/2) \|\mathcal{P}_s^n|_{\tilde{\mathcal{D}}_{\beta,1}}\|_{\beta,1} f \, dx \\ &\le \lim_{n\to\infty} 2^n \|\mathcal{P}_s^n|_{\tilde{\mathcal{D}}_{\beta,1}}\|_{\beta,1} \cdot \|U_s g_0 - g_0/2\|_{s,1} \\ &\le \lim_{n\to\infty} 2^n \cdot C \cdot 4^{-\beta n} (\|U_s\|_{s,1} + 1/2) \|g_0\|_{s,1} = 0 \qquad \text{by Lemma 4}\end{aligned}$$

□

The remaining results are required for the proof of Proposition 2, stated later in this section. Let π_n denote the canonical projection from $\mathcal{B}([0,1]^2)$ onto $\mathrm{sp}\{\chi_{A_1}, \ldots, \chi_{A_{R(n)}}\}$ defined by

$$\pi_n h = \sum_{i=1}^{R(n)} \frac{1}{m(A_i)} \left(\int_{A_i} h \, dm \right) \chi_{A_i}. \tag{17}$$

We describe the matrix representation of $\pi_n U$ on $\mathrm{sp}\{\chi_{A_1}, \ldots, \chi_{A_{R(n)}}\}$.

Lemma 5. *Let $\{A_1, \ldots, A_{R(n)}\}$ partition $M \subset \mathbb{R}^m$ and let $U : L^\infty(M, m) \circlearrowleft$ denote the Koopman operator for a Borel measurable map $T : M \circlearrowleft$. Then*

$$\pi_n U \left(\sum_{i=1}^{R(n)} a_i \chi_{A_i} \right) = \sum_{i=1}^{R(n)} \left(\sum_{j=1}^{R(n)} a_j \frac{m(A_i \cap T^{-1} A_j)}{m(A_i)} \right) \chi_{A_i}.$$

and under left multiplication the matrix representation of $U_n := \pi_n U$ on the space $\mathrm{sp}\{\chi_{A_1}, \ldots, \chi_{A_{R(n)}}\}$ is $P_n^\top$, where P_n is defined by (13).

The proof is included below for completeness; see Li [19] for the corresponding result for the Perron-Frobenius operator $\mathcal{P}$.

Proof.

$$\begin{aligned}
\pi_n U\left(\sum_{i=1}^{R(n)} a_i\chi_{A_i}\right) &= \sum_{i=1}^{R(n)} a_i \pi_n U\chi_{A_i} \\
&= \sum_{i=1}^{R(n)} a_i \sum_{j=1}^{R(n)} \left(\frac{1}{m(A_j)}\int_{A_j} U\chi_{A_i}\, dm\right)\chi_{A_j} \\
&= \sum_{i=1}^{R(n)} a_i \sum_{j=1}^{R(n)} \left(\frac{1}{m(A_j)}\int_{A_j} \chi_{T^{-1}A_i}\, dm\right)\chi_{A_j} \\
&= \sum_{i=1}^{R(n)}\sum_{j=1}^{R(n)} a_i \frac{m(A_j\cap T^{-1}A_i)}{m(A_j)}\chi_{A_j}
\end{aligned}$$

Interchanging i and j we have the result. □

For our particular interval map T_s defined in (9), we will compute left eigenvectors u_n of the matrix $U_{n,s}$ with eigenvalue $1/2$ on the subspace $\mathrm{sp}\{\chi_{I_1},\ldots,\chi_{I_{P(n)}}\}$. The eigenvectors define piecewise constant functions which we show approximate the eigendistribution $\tilde{g}$ of U_s in the $\|\cdot\|_{s,1}$ norm.

Proposition 2. *Let* $\{I_1,\ldots,I_{P(n)}\} = \bigvee_{k=0}^{n} T_s^{-k}\mathfrak{P}_0$ *where* $\mathfrak{P}_0 = \{[0,1/8),[1/8,2/8),\ldots,[7/8,1]\}$. *For each* n, *construct*

$$P_{n,s,ij} = \frac{m(I_i\cap T_s^{-1}I_j)}{m(I_i)} \tag{18}$$

and compute the corresponding right eigenvector u_n *for the eigenvalue* $\lambda_n = 1/2$. *Construct the function* $\hat{g}_n(x) := \sum_{j=1}^{n} u_{n,j}\chi_{I_j}(x)$. *If* u_n *is suitably normalized, then* $\hat{g}_n(x) = g_n(x)$, *and thus* $\hat{g}_n \to \tilde{g}$, *where* g_n *and* $\tilde{g}$ *are defined in Lemma 2.*

Proof of Proposition 2. Construct an eight-symbol symbolic dynamics based on the partition $\mathfrak{P}_0 = \{[0,1/8),[1/8,2/8),\ldots,[7/8,1]\} := \{I_1,I_2,\ldots,I_8\}$. The topological dynamics induced by T_s on these subintervals is described by a subshift of finite type governed by the adjacency matrix

$$A = \begin{pmatrix}
1&1&1&1&0&0&0&0\\
1&1&1&1&0&0&0&0\\
1&1&1&1&0&0&0&0\\
0&0&0&0&1&1&1&1\\
1&1&1&1&0&0&0&0\\
0&0&0&0&1&1&1&1\\
0&0&0&0&1&1&1&1\\
0&0&0&0&1&1&1&1
\end{pmatrix}. \tag{19}$$

As usual, let the cylinder $[i_0\cdots i_n]$ denote the set $I_{i_0}\cap\cdots\cap T_s^{-n}I_{i_n}$. As in Lemma 2, define $g_n = 2^n U_s^n g_0$. Since $g_n(x) = 2^n g_0(T_s^n x)$, and $T_s^n([i_0\cdots i_n]) = [i_n]$,

$$g_n(x) = \begin{cases} 2^n, & \text{if } x\in[i_0\cdots i_n] \text{ and } i_n\in\{1,2,3,5\};\\ -2^n, & \text{if } x\in[i_0\cdots i_n] \text{ and } i_n\in\{4,6,7,8\}.\end{cases}$$

Define $u_{n,i} := g_n(x)$ for $x\in[(i-1)/(2\times 4^n), i/(2\times 4^n))$, $i = 1,\ldots,2\times 4^n$. We now show that u_n is a left eigenvector of $U_{n,s}$. Each index $i = 1,\ldots,2\times 4^n$ represents

a cylinder set of length $n+1$. Consider the cylinder $[i_0 \cdots i_n]$. Then with a slight abuse of notation,

$$(u_n U_{n,s})_{[i_0 \cdots i_n]} = \sum_{a \in \{1,\ldots,8\}, A_{i_n a}=1} u_{n,[i_1 \cdots i_n a]}/4. \tag{20}$$

There are two cases to consider: firstly, $i_n \in \{1,2,3,5\}$, so that three of the allowed $u_{n,[i_1 \cdots i_n a]}$ equal 2^n and the remaining one equals -2^n; in this case, the sum (20) is 2^{n-1}, namely $u_{n,[i_0 \cdots i_n]}/2$; secondly, $i_n \in \{4,6,7,8\}$, so that three of the allowed $u_{n,[i_1 \cdots i_n a]}$ equal -2^n and the remaining one equals 2^n; again in this case, the sum (20) is -2^{n-1}, namely $u_{n,[i_0 \cdots i_n]}/2$. Thus, we have shown that $u_n U_{n,s} = u_n/2$, and so $\hat{g}_n = g_n$. By Lemma 2, $\|\hat{g}_n - \tilde{g}\|_{s,1} \to 0$.

□

We can now prove Theorem 3.

Proof of Theorem 3. Consider the partition $\{I_1, \ldots, I_{P(n)}\}$ of [0,1] from Theorem 3. By Proposition 2, we have a sequence of eigenvectors u_n and step functions $\hat{g}_n(x) = \sum_{i=1}^n u_{n,i} \chi_{I_i}(x)$ satisfying $\hat{g}_n \to \tilde{g} \in \mathcal{B}([0,1])$. Now

$$\begin{aligned} \pi_n \mathcal{P}(\mathbf{1}(y) \cdot \hat{g}_n(x)) &= \pi_n(\mathbf{1}(y) \cdot U_s \hat{g}_n(x)) \qquad \text{by (8)} \\ &= \mathbf{1}(y) \cdot \pi_n^s(U_s \hat{g}_n) \\ &= \mathbf{1}(y) \cdot \hat{g}_n(x)/2, \end{aligned}$$

where π_n^s is the canonical projection onto $\mathrm{sp}\{\chi_{I_1}, \ldots, \chi_{I_{P(n)}}\}$. So $\hat{h}_n(x,y) := \mathbf{1}(y) \cdot \hat{g}_n(x)$ is an eigenfunction of $\pi_n \mathcal{P}$ with eigenvalue $1/2$. By Proposition 2 $\|\hat{h}_n - \tilde{h}\| = \|\mathbf{1} \cdot \hat{g}_n - \mathbf{1} \cdot \tilde{g}\| = b\|\hat{g}_n - \tilde{g}\|_{s,1} \to 0$. □

Acknowledgements. The author is grateful to an anonymous referee for pointing out a simpler approach to proving Theorem 1 in an earlier version of this manuscript, and for discussions with Rua Murray. He thanks Mirko Hessel-von Molo, Oliver Junge, Kathrin Padberg, Stefan Sertl, and Bianca Thiere for assistance with GAIO.

REFERENCES

[1] Viviane Baladi. Unpublished, 1989.
[2] Viviane Baladi and Masato Tsujii. Anisotropic Hölder and Sobolev spaces for hyperbolic diffeomorphisms. Preprint, 2005.
[3] Viviane Baladi and Lai-Sang Young. On the spectra of randomly perturbed expanding maps. *Communications in Mathematical Physics*, 156(2):355–385, 1993.
[4] Michael Blank and Gerhard Keller. Random perturbations of chaotic dynamical systems: stability of the spectrum. *Nonlinearity*, 11:1351–1365, 1998.
[5] Michael Blank, Gerhard Keller, and Carlangelo Liverani. Ruelle-Perron-Frobenius spectrum for Anosov maps. *Nonlinearity*, 15:1905–1973, 2002.
[6] F. Brini, S. Siboni, G. Turchetti, and S. Vaienti. Decay of correlations for the automorphism of the torus $\mathbb{T}^2$. *Nonlinearity*, pages 1257–1268, 1997.
[7] P. Collet and J.-P. Eckmann. Liapunov multipliers and decay of correlations in dynamical systems. *Journal of Statistical Physics*, 115(1/2):217–253, 2004.
[8] Michael Dellnitz, Gary Froyland, and Stefan Sertl. On the isolated spectrum of the Perron-Frobenius operator. *Nonlinearity*, 13:1171–1188, 2000.
[9] Michael Dellnitz and Oliver Junge. On the approximation of complicated dynamical behaviour. *SIAM Journal for Numerical Analysis*, 36(2):491–515, 1999.
[10] Jiu Ding and Aihui Zhou. Finite approximations of Frobenius-Perron operators. a solution of Ulam's conjecture to multi-dimensional transformations. *Physica D*, 92(1–2):61–68, 1996.
[11] Gary Froyland. Finite approximation of Sinai-Bowen-Ruelle measures for Anosov systems in two dimensions. *Random and Computational Dynamics*, 3(4):251–263, 1995.

[12] Gary Froyland. Computer-assisted bounds for the rate of decay of correlations. *Communications in Mathematical Physics*, 189:237–257, 1997.
[13] Gary Froyland and Michael Dellnitz. Detecting and locating near-optimal almost-invariant sets and cycles. *SIAM J. Sci. Comput.*, 24(6):1839–1863, 2003.
[14] Sébastien Gouëzel and Carlangelo Liverani. Banach spaces adapted to Anosov systems. *Ergodic Theory and Dynamical Systems*, 26:189–217, 2006.
[15] Hiroshi Hasegawa and William Saphir. Unitarity and irreversibility in chaotic systems. *Physical Review A*, 46(12):7401–7423, 1992.
[16] Franz Hofbauer and Gerhard Keller. Ergodic properties of invariant measures for piecewise monotonic transformations. *Mathematische Zeitschrift*, 180:119–140, 1982.
[17] Gerhard Keller and Hans Henrik Rugh. Eigenfunctions for smooth expanding circle maps. *Nonlinearity*, 17:1723–1730, 2004.
[18] Andrzej Lasota and Michael C. Mackey. *Chaos, Fractals, and Noise: Stochastic Aspects of Dynamics*, volume 97 of *Applied Mathematical Sciences*. Springer-Verlag, New York, 2nd edition, 1994.
[19] Tien-Yien Li. Finite approximation for the Frobenius-Perron operator. a solution to Ulam's conjecture. *Journal of Approximation Theory*, 17:177–186, 1976.
[20] Prashant Mehta. Personal communication, 2005.
[21] A. Pikovsky and O. Popovych. Persistent patterns in deterministic mixing flows. *Europhys. Lett.*, 61(5):625–631, 2003.
[22] David Ruelle. The thermodynamic formalism for expanding maps. *Commun.Math. Phys.*, 125:239–262, 1989.
[23] Marek Rychlik. Bounded variation and invariant measures. *Studia Mathematica*, 76:69–80, 1983.
[24] Christof Schütte, Wilhelm Huisinga, and Peter Deuflhard. Transfer operator approach to conformational dynamics in biomolecular systems. In Bernold Fiedler, editor, *Ergodic Theory, Analysis, and Efficient Simulation of Dynamical Systems*, pages 191–223. Springer, Berlin, 2001.
[25] S. Ulam. *Problems in Modern Mathematics*. Interscience, 1964.
[26] Joachim Weber, Fritz Haake, Petr A Braun, Christopher Manderfeld, and Petr Seba. Resonances of the Frobenius-Perron operator for a Hamiltonian map with a mixed phase space. *Journal of Physics A*, 34:7195–7211, 2001.

Received February 2006; revised July 2006.

E-mail address: g.froyland@unsw.edu.au